Long-Term Effects of Neonatal Hypoxia-Ischemia on Structural and Physiological Integrity of the Eye and Visual Pathway by Multimodal MRI

Kevin C. Chan,[1–7] Swarupa Kancherla,[1] Shu-Juan Fan,[6,7] and Ed X. Wu[6,7]

[1]UPMC Eye Center, Ophthalmology and Visual Science Research Center, Department of Ophthalmology, School of Medicine, University of Pittsburgh, Pittsburgh, Pennsylvania, United States
[2]Department of Bioengineering, Swanson School of Engineering, University of Pittsburgh, Pittsburgh, Pennsylvania, United States
[3]McGowan Institute for Regenerative Medicine, University of Pittsburgh, Pittsburgh, Pennsylvania, United States
[4]Louis J. Fox Center for Vision Restoration, University of Pittsburgh, Pittsburgh, Pennsylvania, United States
[5]Center for the Neural Basis of Cognition, University of Pittsburgh and Carnegie Mellon University, Pittsburgh, Pennsylvania, United States
[6]Laboratory of Biomedical Imaging and Signal Processing, The University of Hong Kong, Pokfulam, Hong Kong SAR, China
[7]Department of Electrical and Electronic Engineering, The University of Hong Kong, Pokfulam, Hong Kong SAR, China

Correspondence: Kevin C. Chan, Departments of Ophthalmology and Bioengineering, University of Pittsburgh, 3025 East Carson Street, Room 159, Pittsburgh, PA 15203, USA; chuenwing.chan@fulbrightmail.org.

Submitted: March 3, 2014
Accepted: November 24, 2014

Citation: Chan KC, Kancherla S, Fan S-J, Wu EX. Long-term effects of neonatal hypoxia-ischemia on structural and physiological integrity of the eye and visual pathway by multimodal MRI. *Invest Ophthalmol Vis Sci*. 2015;56:1–9. DOI:10.1167/iovs.14-14287

Purpose. Neonatal hypoxia-ischemia is a major cause of brain damage in infants and may frequently present visual impairments. Although advancements in perinatal care have increased survival, the pathogenesis of hypoxic-ischemic injury and the long-term consequences to the visual system remain unclear. We hypothesized that neonatal hypoxia-ischemia can lead to chronic, MRI-detectable structural and physiological alterations in both the eye and the brain's visual pathways.

Methods. Eight Sprague-Dawley rats underwent ligation of the left common carotid artery followed by hypoxia for 2 hours at postnatal day 7. One year later, T2-weighted MRI, gadolinium-enhanced MRI, chromium-enhanced MRI, manganese-enhanced MRI, and diffusion tensor MRI (DTI) of the visual system were evaluated and compared between opposite hemispheres using a 7-Tesla scanner.

Results. Within the eyeball, systemic gadolinium administration revealed aqueous-vitreous or blood-ocular barrier leakage only in the ipsilesional left eye despite comparable aqueous humor dynamics in the anterior chamber of both eyes. Binocular intravitreal chromium injection showed compromised retinal integrity in the ipsilesional eye. Despite total loss of the ipsilesional visual cortex, both retinocollicular and retinogeniculate pathways projected from the contralesional eye toward ipsilesional visual cortex possessed stronger anterograde manganese transport and less disrupted structural integrity in DTI compared with the opposite hemispheres.

Conclusions. High-field, multimodal MRI demonstrated in vivo the long-term structural and physiological deficits in the eye and brain's visual pathways after unilateral neonatal hypoxic-ischemic injury. The remaining retinocollicular and retinogeniculate pathways appeared to be more vulnerable to anterograde degeneration from eye injury than retrograde, transsynaptic degeneration from visual cortex injury.

Keywords: neonatal hypoxia-ischemia, ocular tissue permeability, visual pathway integrity, contrast-enhanced MRI, diffusion tensor imaging

Neonatal hypoxia-ischemia (HI) is a major cause of brain damage in infants and may result in chronic neurological dysfunctions, including visual impairments.[1–6] Apart from brain damage, HI insult in the immature eye also has been recently suggested to play a significant role in long-term visual impairment.[2,7] Although advancements in perinatal care have increased survival, the pathogenesis of neonatal HI injury and the long-term consequences to the visual system remain unclear, partly because of limited noninvasive tools to monitor the pathophysiological events of HI in the eye and brain systematically. Understanding the chronic effects of neonatal HI on the remaining visual pathways of the survivors are potentially important in determining and improving the functional consequences of HI lesions in the visual system before most compensatory and reparative phases have been passed.

Magnetic resonance imaging (MRI) allows noninvasive, longitudinal, and multiparametric assessments of the visual system without depth limitation. Although clinical studies using conventional MRI often detected cerebral damage in HI-injured infants with impaired visual acuity, the severity could not be predicted solely on brain imaging.[7,8] This suggested the need for more in-depth understanding of the pathogenesis of neonatal HI in the whole visual system. In this study, we

Copyright 2015 The Association for Research in Vision and Ophthalmology, Inc.

developed an in vivo model system using multimodal MRI to determine the pathophysiological events of HI in both the eye and the brain's visual pathways. Our aim was to better understand the basic mechanisms of HI in the visual system and to help guide and assess potential neuroprotective strategies in the future. In recent years, several endogenous[9–13] and exogenous[14–21] MRI contrasts have been developed and applied to study the eye and the visual pathway in healthy and diseased animal models. Within the eyeball, systemic administration of the gadolinium diethylenetriamine pentaacetic acid (Gd-DTPA) MR contrast agent allowed noninvasive assessments of the aqueous humor dynamics and the permeability of the blood-aqueous, aqueous-vitreous, and blood-retinal barriers in different ocular compartments simultaneously in both eyes.[14,15,22–24] Local administration of potassium dichromate ($K_2Cr_2O_7$) and manganese chloride ($MnCl_2$) MR contrast agents may help assess the biochemical properties of the retina and the active axonal transport in the visual pathway.[17,18,20,25–29] Diffusion tensor MR imaging (DTI) probes the anisotropic property of tissue water[30,31] and has been successfully used to reveal the microstructural integrity of the optic nerve and optic tract in normal, developing, and injured brains.[30–35] In this study, we tested the hypothesis that the structural and physiological effects of neonatal HI occur in both the eye and the brain's visual pathways and persist in the long term. High-field anatomical MRI, contrast-enhanced MRI, and DTI metrics were established for assessing the general morphology, ocular physiology, axonal transport, and microstructural integrity of the visual system in adult rats that had undergone unilateral neonatal HI. The relative extents of multimodal MRI changes along the visual pathways were evaluated and compared between opposite hemispheres. Our results demonstrated the use of high-field multimodal MRI as an effective tool to determine in vivo the chronic structural and physiological deficits of the HI-injured visual system. They also indicated the higher susceptibility of the remaining visual pathways in the surviving animals to the spread of degeneration from eye injury over visual cortex injury.

Materials and Methods

Animal Preparation

All animal experiments were performed in accordance with the ARVO Statement for the Use of Animals in Ophthalmic and Vision Research. Sprague-Dawley rats (12–16 g, $n = 8$, Charles River Laboratory, Wilmington, MA, USA) underwent unilateral ligation of the left common carotid artery at postnatal day 7 under isoflurane anesthesia, followed by hypoxia in 8% oxygen and 92% nitrogen at 36 to 37°C for 2 hours.[36] One year after HI insults, T2-weighted imaging and DTI were performed on all animals followed by dynamic gadolinium-enhanced MRI (Gd-MRI) after intraperitoneal injection of the passive Gd-DTPA contrast agent at 3 mmol/kg. One month after DTI and Gd-MRI, chromium-enhanced MRI (Cr-MRI) was performed on four randomly selected animals and manganese-enhanced MRI (Mn-MRI) on the other four animals at 1 day after intravitreal injection of Cr(VI) (3 μL, 10 mM[20]) and $MnCl_2$ (3 μL, 50 mM[27–29]) solutions, respectively into both eyes. Diffusion tensor MR imaging and Gd-MRI were acquired before Cr-MRI and Mn-MRI to avoid any potential toxic effects induced by intravitreal Cr or Mn injection on the visual pathway that might confound DTI and Gd-MRI assessment. On the other hand, Cr-MRI and Mn-MRI were performed 1 month after Gd-MRI to guarantee sufficient time for complete clearance of the passive Gd T1 MR contrast agent from the eye, brain, and body before introducing other exogenous T1 MR contrast agents (i.e., Cr and Mn) into the eye for contrast-enhanced MRI. Because more than 90% of the optic nerve fibers in normal rats cross the optic chiasm to the optic tract of the contralateral hemisphere,[37,38] and that unilateral carotid artery occlusion affected mainly the ipsilateral ophthalmic artery and ipsilateral visual cortex,[7] the visual pathway projected from the ipsilesional left eye from the ipsilesional retina and optic nerve to the contralesional optic tract and visual brain nuclei were largely separated from the visual pathway projected from the contralesional eye to the ipsilesional brain nuclei in the opposite hemispheres. Such a model was used to separate the effects of eye and brain HI injuries on different visual pathways to compare the relative contributions of anterograde degeneration from eye injury and retrograde, transsynaptic degeneration from visual cortex injury to the visual pathways in the same animals.

Magnetic Resonance Imaging Protocols

All MRI measurements were acquired using a 7-Tesla Bruker scanner (Bruker Biospin GmbH, Rheinstetten, Germany) with a maximum gradient of 360 mT/m (70/16 PharmaScan; Bruker Biospin GmbH, Germany), a 72-mm birdcage transmit-only radiofrequency coil, and an actively decoupled receive-only quadrature surface coil. Under inhaled isoflurane anesthesia (3% induction and 1.5% maintenance), animals were kept warm under circulating water at 37°C with continuous monitoring of the respiration rate in the range of approximately 55 to 65 breaths per minute. Scout T2-weighted images were first acquired in three planes with a rapid-acquisition-with-relaxation-enhancement (RARE) pulse sequence to position the subsequent MR images along standard anatomical orientations in a reproducible manner. For DTI, multishot spin-echo echo-planar-imaging diffusion-weighted images were acquired with field-of-view (FOV) = 32 × 32 mm^2, matrix resolution = 128 × 128, slice thickness = 1 mm, number of slices = 12, repetition time (TR)/echo time (TE) = 3000/30 ms, b-value = 0 and 1000 s/mm^2, diffusion time (Δ) = 15 ms, diffusion gradient duration (δ) = 5 ms, number of shots = 4, and 30 diffusion directions. For Gd-MRI, two-dimensional (2D) T1-weighted RARE images were acquired within the first 60 minutes after Gd administration, with TR/TE = 320/10.4 ms, RARE factor = 4, number of averages = 20, FOV = 32.7 × 32.7 cm^2, voxel resolution = 64 × 64 μm^2, and slice thickness = 1 mm. Chromium-enhanced MRI and Mn-MRI were performed using 2D T1-weighted RARE sequences covering the eye and the brain with TR/TE = 475/8.8 ms, RARE factor = 4, number of averages = 26, FOV = 32 × 32 cm^2, voxel resolution = 125 × 125 μm^2, and slice thickness = 0.5 mm. Three-dimensional T1-weighted imaging also was acquired covering the entire visual pathway using modified driven equilibrium Fourier transform (MDEFT) imaging sequence with TR = 2500 ms, echo TR/TE = 9/3 ms, inversion time = 1200 ms, number of segments = 1, number of averages = 8, FOV = 32 × 32 mm^2, voxel resolution = 200 × 200 μm^2, slice thickness = 0.24 mm, and number of slices = 46.

Data Analysis

The general morphology of the eye and the brain was qualitatively evaluated in anatomical T2-weighted imaging in all animals. The T1-weighted signal intensities in the anterior chamber and vitreous body of each eye in Gd-MRI,[23,24] in the retina of each eye in Cr-MRI,[20] and in the optic nerve and superior colliculus of each hemisphere in Mn-MRI[27,28] were measured using ImageJ v1.43u (http://imagej.nih.gov/ij/; provided in the public domain by the National Institutes of Health, Bethesda, MD, USA) based on the anatomical landmarks in the

Investigative Ophthalmology & Visual Science

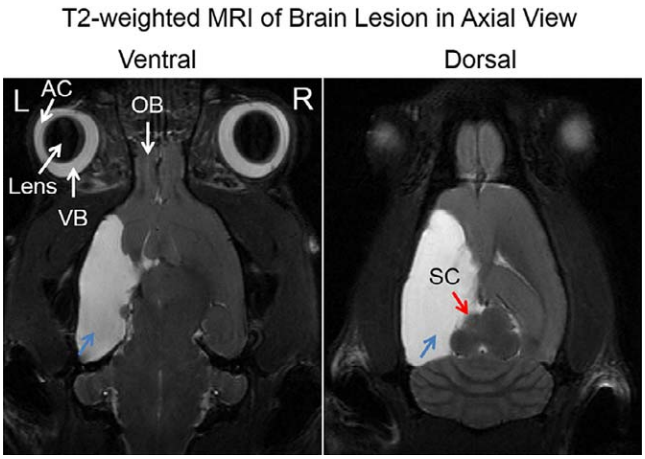

Figure 1. Axial T2-weighted MRI of the adult rat brain, showing the extent of cystic lesions in the left cortical hemisphere (*blue arrows*) at 1 year after unilateral neonatal hypoxic-ischemic injury at postnatal day 7. Note also the smaller left superior colliculus (*red arrow*) compared with the right hemisphere. AC, anterior chamber; VB, vitreous body; OB, olfactory bulb.

MR images and the rat brain atlas.[39] We calculated the relative signal enhancement of Gd and Cr via dividing the signal intensity at each time point by that at the earliest time point acquired. For Mn-MRI, the T1-weighted signal intensities were normalized to the surrounding muscles. For DTI, color-encoded fractional anisotropy (FA) directionality map and DTI parametric maps (FA value, axial diffusivity [$\lambda_{//}$], radial diffusivity [$\lambda_{\perp}$], and mean diffusivity [MD] maps) were obtained using DTIStudio v2.30 (Johns Hopkins University, Baltimore, MD, USA) after coregistration using AIR v5.2.5 (Roger Woods, University of California Los Angeles, Los Angeles, CA, USA). Manual segmentation was performed to the FA maps along the prechiasmatic optic nerve, and the anterior and posterior optic tracts using ImageJ in accordance with the rat brain atlas.[39] Identical region-of-interest definitions of the white matter components on FA maps were applied to $\lambda_{//}$, $\lambda_{\perp}$, and MD maps for measurements. All extracted Gd-MRI, Cr-MRI, Mn-MRI, and DTI parametric values were presented as mean ± SD. The time courses of Gd-MRI of both eyes were evaluated using ANOVA followed by post hoc Dunnett's tests between each time point and the first time point to counter for potential Type I errors from multiple comparisons. Chromium-enhanced MRI, Mn-MRI, and DTI were compared between opposite hemispheres using two-tailed paired *t*-tests. Results were considered significant when P was less than 0.05.

Results

Morphologically, in all adult rats receiving unilateral neonatal HI injury to the left hemisphere, a large cyst was observed covering most of the left posterior cortical brain including the visual cortex in anatomical T2-weighted images (Fig. 1), whereas the eyes and the subcortical visual nuclei, such as the superior colliculus, appeared generally comparable between opposite hemispheres (Fig. 1).

Within the eyeball, after systemic administration of the passive Gd tracer, Gd signal intensities in T1-weighted imaging were continuously enhanced at similar rates in the anterior chamber of both eyes up to approximately 70% signal increase by the end of the 1-hour experimental period (ANOVA, $P < 0.0001$; post hoc Dunnett's tests with first time point, $P < 0.01$) (Figs. 2a, 2b). In the vitreous body, weaker but significant Gd enhancement was observed only in the ipsilesional left eye by approximately 14% to 18% (ANOVA, $P < 0.05$; post hoc Dunnett's tests with first time point, $P < 0.01$) but not the contralesional right eye (ANOVA, $P > 0.05$) at the later time points (Figs. 2a, 2c). Specifically, the anterior portion of the left vitreous appeared to enhance earlier starting at approximately 40 minutes post Gd administration as compared with the posterior portion of the left vitreous at 60 minutes post Gd administration (Fig. 2c).

After intravitreal injection of the exogenous Cr and Mn contrast agents to both eyes, Cr-MRI of the retina showed a 16% smaller T1-weighted signal increase in the ipsilesional left eye than the contralesional right eye at 1 day post Cr administration (paired *t*-test, $P < 0.05$) (Fig. 3). Along the visual pathway, Mn-MRI showed more enhancement of the active Mn anterograde transport tracer in the left vitreous, left retina, right optic nerve, left superior colliculus, and left lateral geniculate nucleus as compared with the opposite hemispheres (Fig. 4). Regions-of-interest–based Mn-MRI analysis showed that the ipsilesional left prechiasmatic optic nerve possessed lower Mn-enhanced signal intensity than the contralesional right optic nerve by approximately 14% (paired *t*-test, $P < 0.05$), whereas the contralesional right superior colliculus possessed 23% lower Mn-enhanced signal intensity than the ipsilesional left superior colliculus (paired *t*-test, $P < 0.05$) (Fig. 4b). As needle insertion and material injection in the eye might induce reactive changes in the retina and possibly the visual system, to address the potential issue of "injection artifact," we also compared the current Cr-MRI and Mn-MRI data from the HI-injured animals with healthy control animals from our previous data using the same MRI acquisition parameters, the same Cr or Mn dose, and the same time points before and after Cr or Mn injection.[20,29] For Cr-MRI, no significant difference was observed between HI-injured animals and healthy animals on either side of the retina before Cr injection (unpaired *t*-tests, $P > 0.05$). One day after Cr injection, the Cr enhancement in the retina of the healthy animals was significantly stronger than the ipsilesional left retina (unpaired *t*-test, $P < 0.05$) but not contralesional right retina (unpaired *t*-test, $P > 0.05$) of the HI-injured animals. For Mn-MRI, the Mn enhancement in the superior colliculus of healthy animals had no apparent difference compared with the ipsilesional left superior colliculus of the HI-injured animals (unpaired *t*-test, $P > 0.05$) , but was significantly stronger than the contralesional right superior colliculus of the HI-injured animals at 1 day after Mn injection to both eyes (unpaired *t*-test, $P < 0.05$). Taken together, we conclude that the "injection artifacts" did not appear to contribute significantly to the differences in Cr or Mn enhancements between opposite hemispheres of the rat model of unilateral neonatal HI in this study.

By examining the DTI parametric values along the visual pathway, the ipsilesional prechiasmatic optic nerve possessed significantly lower FA, higher $\lambda_{\perp}$, and higher MD than the contralesional optic nerve by 56%, 90%, and 48%, respectively (paired *t*-tests, $P < 0.01$). After the optic nerve fibers decussated at the optic chiasm to the opposite hemispheres, the contralesional anterior optic tract possessed 26% lower FA than the ipsilesional anterior optic tract (paired *t*-test, $P < 0.05$), whereas the contralesional posterior optic tract possessed 38% lower $\lambda_{//}$ than the ipsilesional posterior optic tract (paired *t*-test, $P < 0.01$) (Fig. 5).

Discussion

The results of this study supported the hypothesis that the structural and physiological effects of neonatal HI injury

Investigative Ophthalmology & Visual Science

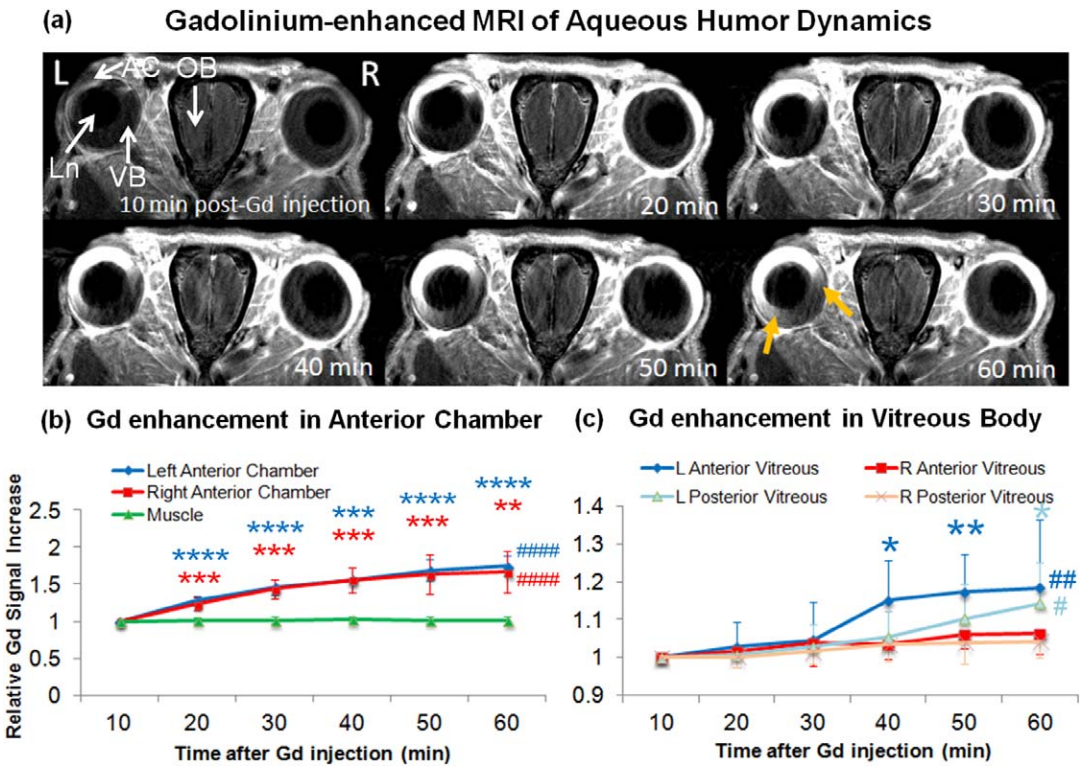

Figure 2. (**a**) Dynamic T1-weighted MRI of aqueous humor dynamics at 10 to 60 minutes after intraperitoneal injection of Gd contrast agent, showing rapid Gd enhancement in the AC of both eyes via the highly permeable blood-aqueous barrier. In the ipsilesional left eye, there was a slow, gradual increase in Gd enhancement in the anterior portion of the VB (*yellow arrows*). Such enhancement was not apparent in the contralesional right anterior vitreous body, suggestive of the compromise of aqueous-vitreous or blood-ocular barrier in the ipsilesional eye. Ln, lens. (**b**, **c**) Time profiles of T1-weighted signal intensities in the anterior chamber and the nearby muscle (**b**), and in the anterior and posterior VB (**C**) relative to the first time point after systemic Gd administration. Gd signals continuously enhanced in the anterior chamber of both eyes at similar rates within the 1-hour experimental period (ANOVA, $\#\#\#\#P < 0.0001$; post hoc Dunnett's tests with first time point, $^{**}P < 0.01$; $^{***}P < 0.001$; $^{****}P < 0.0001$). Significant Gd enhancement also was observed at later time points in the ipsilesional left vitreous but not the contralesional right vitreous (ANOVA, $\#P < 0.05$; $\#\#P < 0.01$; post hoc Dunnett's tests with first time point, $^{**}P < 0.01$; $^{*}P < 0.05$; $^{***}P < 0.001$). The anterior portion of the left vitreous appeared to enhance earlier at approximately 40 minutes post Gd administration than the posterior portion of the left vitreous at 60 minutes post GD administration, suggestive of the compromise of aqueous-vitreous or blood-ocular leakage leading to the Gd flow from the anterior to posterior vitreous. No change in signal intensity was observed in the muscle, or in the contralesional right vitreous (ANOVA, $P > 0.05$).

persisted chronically in both the eye and brain's visual pathway of the surviving animals and can be revealed with high-field, in vivo multimodal MRI. In the ipsilesional hemisphere of adult rats that had undergone unilateral neonatal HI injury, T2-weighted imaging demonstrated cystic lesions in the posterior cortical brain, including the visual cortex. Despite generally comparable eye morphology in T2-weighted imaging, Gd-MRI and Cr-MRI showed abnormalities in the ocular tissue barriers and retinal integrity within the eyeball. In the presence of both eye and visual cortex damage, Mn-MRI and DTI indicated that the remaining retinocollicular and retinogeniculate pathways appeared to be more vulnerable to anterograde degeneration from eye injury than retrograde, transsynaptic degeneration from visual cortex injury. High-field MRI allowed improved sensitivity in detecting eye and brain changes in small animals, whereas in vivo MRI evaluation allowed multimodal and longitudinal assessments to obtain comprehensive and systematic biological information in the eye and the brain without destructive processing from ex vivo studies or invasive procedures that could disrupt normal physiological conditions. Taken together, the results of this study provided an in vivo model system for better understanding the basic mechanisms of neonatal HI in the visual system, which may help monitor and guide neuroprotective strategies to the eye and the brain in the future.

Gadolinium is a Food and Drug Administration–approved passive T1 MR contrast agent and has a low molecular weight. After systemic Gd administration, Gd may mimic soluble aqueous humor components and readily pass the highly permeable blood-aqueous barrier into the anterior chamber but not the less permeable aqueous-vitreous or blood-retinal barrier into the vitreous body.[14,15,22–24] In this study, Gd-MRI showed similar Gd enhancement patterns and comparable aqueous humor dynamics in the anterior chamber of both eyes after unilateral neonatal HI injury. However, significant Gd enhancement was observed in the vitreous body of the ipsilesional eye but not the contralesional eye by the end of the 1-hour Gd-MRI experiment. Specifically, there was an earlier Gd enhancement in the anterior vitreous than the posterior vitreous in the ipsilesional eye in the latter half of the experimental period. These suggested that neonatal HI injury may compromise the permeability at the aqueous-vitreous and/or the blood-ocular barriers, leading to the leakage of Gd into the anterior vitreous flowing to the posterior vitreous. Gd-MRI has been used to reveal underdeveloped tight junctions in the aqueous-vitreous interface of normal neonatal rats reflective of the leakage of proteins from the bloodstream in the ciliary body and iris complex to the vitreous humor in the immature eyes.[22] Because carotid artery occlusion may impair the ophthalmic artery and thus blood supply to the ocular tissues without apparent changes in systemic arterial pressure,[7,40] it is

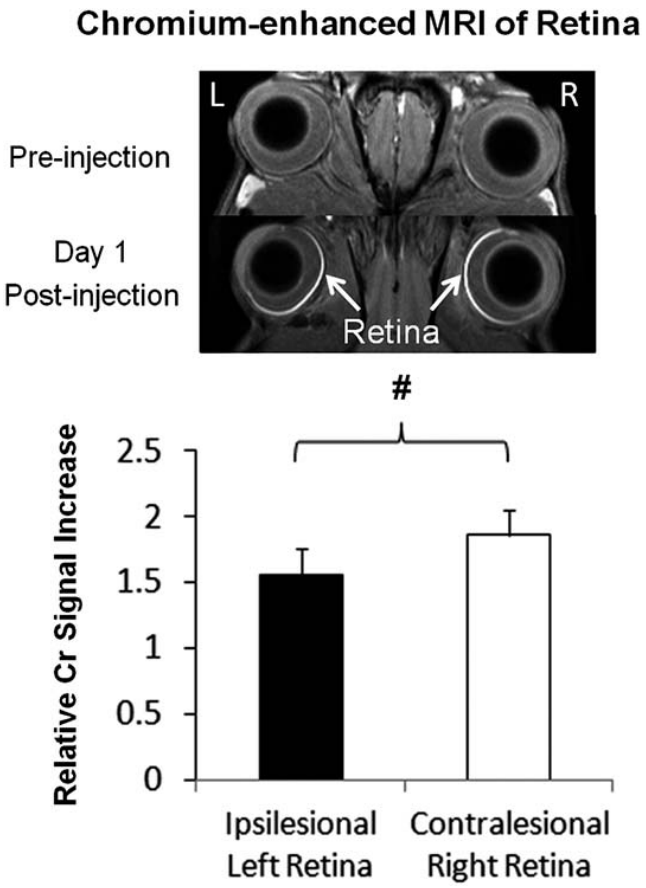

FIGURE 3. *Top*: Chromium-enhanced MRI of the retina before and at 1 day after binocular intravitreal Cr (VI) injection. *Bottom*: Ipsilesional left retina possessed 16% lower Cr-enhanced signal increase than contralesional right retina (two-tailed paired *t*-test, $\#P < 0.05$).

postulated that unilateral HI injury might have altered the normal development of the tight junctions at the aqueous-vitreous interface in the ipsilesional eye of the neonatal rats, leading to the sustained leakage of Gd into the vitreous of the ipsilesional eye but not the contralesional eye in the adult rats. Although it is not clear whether such a change in metabolic environment in the vitreous body from neonatal HI might possess causal effect on the pathogenesis of chronic retinal injury and visual impairment in the adult rats, similar Gd-MRI findings on the compromise of aqueous-vitreous or blood-ocular barrier integrity have been observed in the experimental chronic glaucoma models, whereby the retina and optic nerve fibers of the adult rats were concurrently injured.[23,24] Gadolinium-enhanced MRI has been used to evaluate the efficacy of therapeutic drugs on anterior uveitis across the blood-ocular barriers.[15] Future studies are envisioned that elucidate the relations of ocular tissue permeability to retinal health and visual function. Future studies also may determine whether Gd-MRI can help assess treatment strategies to the HI-injured eye by monitoring changes in aqueous humor flow and the integrity of ocular tissue permeability.

Recent studies have suggested the potential linkage between Cr contrast and lipid metabolism in the retina and the brain in Cr-MRI.[20,41–43] In the eye, lipid peroxidation may play an important role in degenerative diseases, such as AMD, cataract, glaucoma, retinopathy of prematurity, and diabetic retinopathy.[44] Chromium-enhanced MRI may provide an in vivo biomarker to help determine the pathophysiological and pharmacological implications of lipid peroxidation in the injured eye, as peroxides and metabolites of long-chain polyunsaturated fatty acids in the retina may alter the integrity of neurotransmitter pools and provide new potential target sites and pathways for the treatment of degenerative ocular diseases.[44] After neonatal HI injury, severe hypoxic stress could be induced in ganglia cells leading to apoptotic neuronal death in the inner retina.[7] Cellular lipids in the outer retina may also be altered by oxidative stress on HI insults.[45] In the current study, although there was no apparent difference in T1-weighted signal intensities between bilateral retinas before Cr

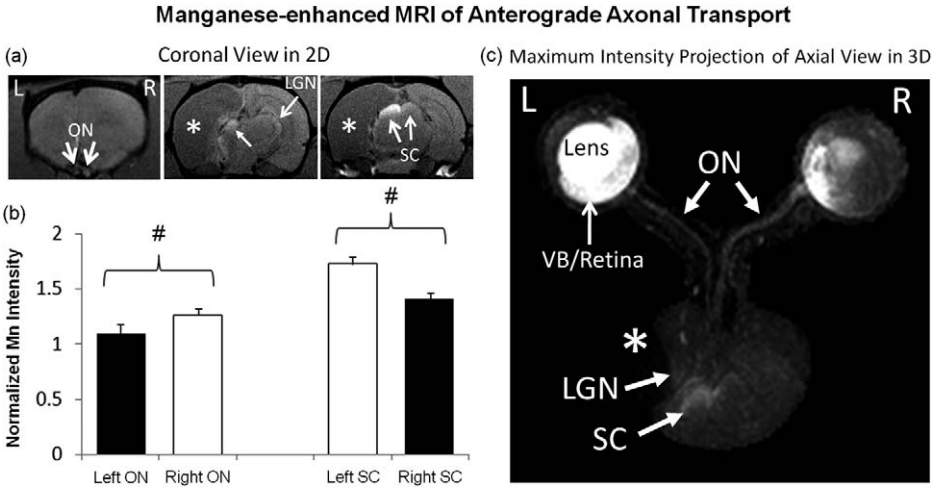

FIGURE 4. Manganese-enhanced MRI of anterograde axonal transport along the visual pathways at 1 day after binocular intravitreal Mn^{2+} injection in 2D multislice coronal view (**a**) and 3-dimensional maximum-intensity-projected axial view (**c**). Qualitatively, more Mn enhancement was observed in left VB, left retina, right optic nerve (ON), left superior colliculus (SC), and left lateral geniculate nucleus (LGN) as compared with the opposite hemispheres. The ipsilesional LGN also appeared to be slightly displaced by the cystic lesion in the cortex. Quantitative analysis in (**b**) showed 14% lower Mn enhancement in the ipsilesional left ON than the right contralesional ON (two-tailed paired *t*-test, $\#P < 0.05$), whereas the left ipsilesional SC possessed 23% stronger Mn enhancement than the right contralesional SC (two-tailed paired *t*-test, $\#P < 0.05$). *Black bars* refer to visual pathway projected from the ipsilesional eye to ipsilesional ON and contralesional SC. *White bars* refer to visual pathway projected from the contralesional eye to the contralesional ON and ipsilesional SC. *Asterisks* indicate hypointense brain lesion in cortical regions.

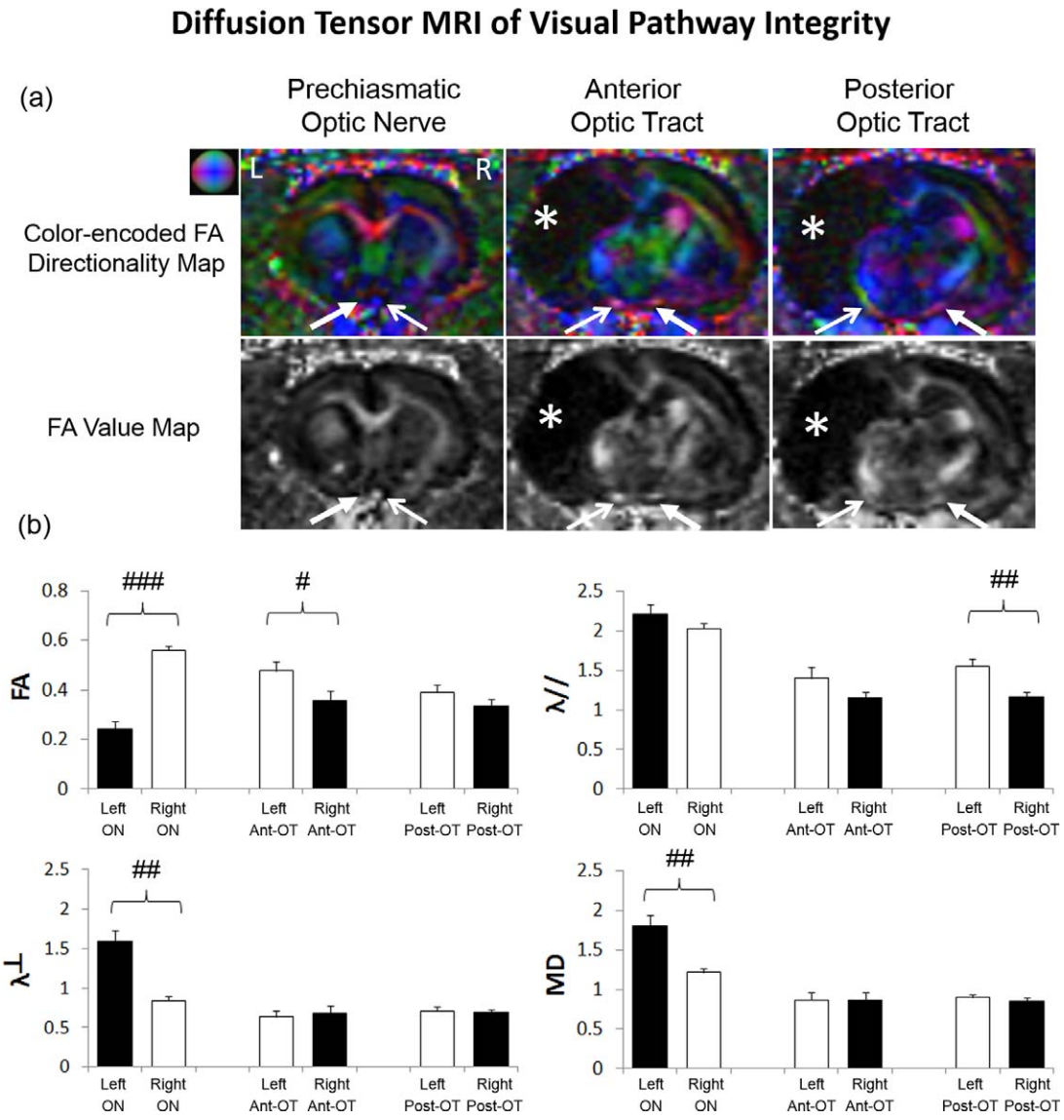

Figure 5. Diffusion tensor MRI (DTI) of structural integrity in the prechiasmatic ON, anterior optic tract (OT), and posterior OT at 1 year after unilateral neonatal hypoxic-ischemic injury at postnatal day 7. (**a**) Color-encoded fractional anisotropy (FA) directionality maps and FA value maps in coronal view showed lower FA in the ipsilesional left ON than the contralesional right ON. The contralesional right anterior OT projected from ipsilesional left eye also had apparently lower FA than the opposite hemisphere. (Representative colors for different directions in color-encoded FA directionality map: *blue*, caudal-rostral; *red*, left-right; and *green*, dorsal-ventral; *closed arrows*, visual pathway projected from ipsilesional eye to ipsilesional ON and contralesional OT; *open arrow*, visual pathway projected from the contralesional eye to the contralesional ON and ipsilesional OT; *white asterisks*, brain lesion.) (**b**) Quantitative analysis of DTI-derived parameters in the prechiasmatic ON, anterior OT (Ant-OT), and posterior optic tract (Post-OT) of the ipsilesional left and contralesional right hemispheres. The ipsilesional prechiasmatic ON possessed 56% lower FA, 90% higher radial diffusivity ($\lambda_{\perp}$) and 48% higher mean diffusivity (MD) than the contralesional ON (two-tailed paired *t*-tests, $\#\#P < 0.01$; $\#\#\#P < 0.001$). The contralesional anterior OT possessed 26% lower FA than the opposite hemisphere (two-tailed paired *t*-test, $\#P < 0.05$). The contralesional posterior OT possessed 38% lower axial diffusivity ($\lambda_{//}$) than the opposite hemisphere (two-tailed paired *t*-test, $\#\#P < 0.01$). *Black bars* refer to visual pathway projected from the ipsilesional eye to ipsilesional ON and contralesional OT. *White bars* refer to visual pathway projected from the contralesional eye to the contralesional ON and ipsilesional OT. Units for $\lambda_{//}$, $\lambda_{\perp}$, and MD: μm^2/ms; no unit for FA.

administration, weaker Cr enhancement was observed in the ipsilesional retina compared with the contralesional retina at 1 day after binocular intravitreal Cr injection. This likely reflected compromised retinal integrity in the ipsilesional eye. Although decrease in chromium binding to the retina may suggest altered lipid peroxidation, other factors, such as decreased cellularity, retinal thinning, and partial volume effect from limited imaging spatial resolution in the current study, may cofound chromium-enhanced signal intensity changes in the retina. The exact pathophysiological events contributive to the Cr-MRI differences between bilateral retinas require detailed histological evaluations and high-resolution MRI using specialized hardware settings and will be the subject of future investigation. However, the current Gd-MRI and Cr-MRI findings provided substantial evidence to concur with recent reports suggesting that HI injury caused long-lasting impairments in the ocular integrity apart from visual brain damage.[7]

In HI-injured children, the loss of visual function has often been attributed to cerebral visual impairment, and the optic nerve axons are thought to be predominantly injured by

Investigative Ophthalmology & Visual Science

transsynaptic degeneration from occipital brain damage, as the eyes are presumed to be more resistant than the brain after HI injury.[7,46] After binocular intravitreal injection of the active Mn tracer to our rat model, weaker Mn enhancement was observed in the ipsilesional optic nerve and the contralesional superior colliculus and lateral geniculate nucleus compared with the opposite hemispheres. This indicated reduced anterograde Mn transport along the retinocollicular and retinogeniculate visual pathways projected from the ipsilesional eye, whereas the axoplasmic Mn transport along the retinal pathways projected from the contralesional eye to the ipsilesional superior colliculus and lateral geniculate nucleus appeared to be spared despite cystic formation and total loss of the ipsilesional visual cortex, as shown in T2-weighted imaging. Our DTI results also revealed more pronounced FA decrease along the anterior visual pathways projected from the ipsilesional eye (i.e., ipsilesional left optic nerve and contralesional right anterior optic tract) compared with those projected from the contralesional eye, whereas no apparent FA difference was observed in posterior optic tracts between hemispheres. The DTI-derived parameters, namely FA, $\lambda_{//}$, and $\lambda_{\perp}$, have been shown to be sensitive to the overall microstructural integrity, axonal integrity, and myelin integrity, respectively, in the white matter.[30,31,33] At the same time, recent studies suggested that acute and chronic inflammation also may contribute to changes in FA, $\lambda_{//}$, and $\lambda_{\perp}$ in the neural pathways.[47–49] Although the current DTI study did not determine the exact pathophysiological events occurring along the HI-injured visual pathway, by comparing the extents of overall Mn-MRI and DTI differences between hemispheres, our findings suggested that the remaining retinocollicular and retinogeniculate pathways could be more vulnerable to anterograde degeneration from eye injury than the retrograde, transsynaptic degeneration from visual cortex injury after unilateral neonatal HI in our rat model. Recent evidence showed that the primary visual cortex in rat is required for detecting image orientation and motion discrimination.[50] The relatively intact contralesional visual cortex and the residual Mn transport and neural connections along the visual pathway projected from the ipsilesional eye in our rat model may offer a potential site for testing behavioral outcomes involving higher-order visual processing in the visual cortex after predominant visual pathway injury spreading from the eye. Although visual cortical brain damages can lead to retrograde, transsynaptic degeneration in the visual pathways,[51–53] some retinogeniculate and retinocollicular projections can be sustained in the absence of transneuronal relay cells after visual cortical damage,[54] and the subcortical visual nuclei may remain responsive to visual stimulation after neonatal HI injury.[36,55,56] Despite the absence of subcortical-cortical connections due to total loss of the ipsilesional visual cortex, the relatively spared axoplasmic flow and structural integrity of the retinocollicular and retinogeniculate pathways projected from the contralesional eye in the current animal model may be helpful in examining residual visual functions that are mainly mediated by the subcortical visual nuclei, such as blindsight.[55,57–60]

Although our current MRI data supported the hypothesis that both the eye and the brain's visual pathway were affected by neonatal HI, it is currently uncertain the relative contributions of altered structural and physiological integrity in the visual system to visual impairment. Vision testing was not performed on the current albino Sprague-Dawley rat model because of the intrinsically low visual acuity of normal albino rats,[61] leaving limited room to quantitatively and reliably assess visual performance impairment and/or recovery. Because the severity of neonatal HI injury of the rat model is dependent on the duration of hypoxia,[7] future studies may use MRI and visuomotor behavioral assessments[61,62] to animal models of neonatal HI using pigmented rodents to evaluate how alterations in structural and physiological MRI characteristics in the eye and brain may reflect psychophysical changes under different hypoxia durations mimicking different pathological conditions of human neonatal HI. It has been suggested that treatment to both the eye and the brain on optic nerve injury may provide better outcomes than treating the eye alone.[63] Given our multimodal MRI observations of the long-lasting compromise in ocular integrity, optic neuropathy, and visual cortex injury on neonatal HI, our current study may provide an in vivo model system to assess the beneficial effects of different neuroprotective strategies on both the eye and the brain in neonatal HI in future studies. Further studies may use more advanced diffusion MRI techniques to better characterize neural tissue alterations within the complex pathophysiological environment along the injured visual pathways.[47–49,64–66] Future studies also may combine the developed imaging techniques here with functional MRI[36,67–70] and proton MR spectroscopy of the visual brain nuclei[71–74] for more in-depth monitoring of the structural-metabolic-functional relationships and the progression of HI in the visual system.

Conclusions

Based on the findings of anatomical MRI, contrast-enhanced MRI, and diffusion tensor MRI in the eye and the brain, we conclude that in animals surviving from severe unilateral neonatal HI injury, the long-term structural and physiological deficits occurred and persisted in both the eye and the brain's visual pathway. In addition, high-field, multiparametric MRI indicated the higher susceptibility of the remaining visual pathways to anterograde degeneration from eye injury than retrograde, transsynaptic degeneration from visual cortex injury. The results of this study provided a foundation for understanding and detecting the chronic pathophysiological changes in the visual system after neonatal unilateral HI injury using recently developed endogenous and exogenous contrasts in high-field MRI. The established MRI metrics on the current animal model here also may be used as an in vivo model system to provide systematic assessments of neonatal hypoxic-ischemic injury and to evaluate neuroprotective strategies in the future, given the advantages of MRI allowing noninvasive, multimodal assessments of the whole eye and brain simultaneously and longitudinally.

Acknowledgments

Supported by National Institutes of Health Core Grant (P30-EY008098) and Cooperative Agreement (UL1-TR000005), Bright-Focus Foundation (G2013077), Alcon Research Institute Young Investigator Grant, Eye and Ear Foundation of Pittsburgh, an unrestricted grant from Research to Prevent Blindness, and Hong Kong Research Grant Council (GRF HKU 7837/11M).

Disclosure: **K.C. Chan**, None; **S. Kancherla**, None; **S.-J. Fan**, None; **E.X. Wu**, None

References

1. Fazzi E, Bova SM, Uggetti C, et al. Visual-perceptual impairment in children with periventricular leukomalacia. *Brain Dev.* 2004;26:506–512.
2. Jacobson L, Ygge J, Flodmark O, Ek U. Visual and perceptual characteristics, ocular motility and strabismus in children with periventricular leukomalacia. *Strabismus.* 2002;10:179–183.
3. Jacobson LK, Dutton GN. Periventricular leukomalacia: an important cause of visual and ocular motility dysfunction in children. *Surv Ophthalmol.* 2000;45:1–13.

4. Ferriero DM. Neonatal brain injury. *N Engl J Med*. 2004;351:1985–1995.
5. Hoyt CS. Brain injury and the eye. *Eye (Lond)*. 2007;21:1285–1289.
6. Luna B, Dobson V, Scher MS, Guthrie RD. Grating acuity and visual field development in infants following perinatal asphyxia. *Dev Med Child Neurol*. 1995;37:330–344.
7. Huang HM, Huang CC, Hung PL, Chang YC. Hypoxic-ischemic retinal injury in rat pups. *Pediatr Res*. 2012;72:224–231.
8. Pike MG, Holmstrom G, de Vries LS, et al. Patterns of visual impairment associated with lesions of the preterm infant brain. *Dev Med Child Neurol*. 1994;36:849–862.
9. Xu J, Sun SW, Naismith RT, Snyder AZ, Cross AH, Song SK. Assessing optic nerve pathology with diffusion MRI: from mouse to human. *NMR Biomed*. 2008;21:928–940.
10. Spees WM, Lin TH, Song SK. White-matter diffusion fMRI of mouse optic nerve. *Neuroimage*. 2013;65:209–215.
11. Duong TQ. Magnetic resonance imaging of the retina: from mice to men. *Magn Reson Med*. 2014;71:1526–1530.
12. Chan KC, Cheung MM, Wu EX. In vivo multiparametric magnetic resonance imaging and spectroscopy of rodent visual system. *J Integr Neurosci*. 2010;9:477–508.
13. Ho LC, Sigal IA, Jan NJ, et al. Magic angle-enhanced MRI of fibrous microstructures in sclera and cornea with and without intraocular pressure loading. *Invest Ophthalmol Vis Sci*. 2014;55:5662–5672.
14. Berkowitz BA, Sato Y, Wilson CA, de Juan E. Blood-retinal barrier breakdown investigated by real-time magnetic resonance imaging after gadolinium-diethylenetriaminepentaacetic acid injection. *Invest Ophthalmol Vis Sci*. 1991;32:2854–2860.
15. Kolodny NH, Goode ST, Ryan W, Freddo TF. Evaluation of therapeutic effectiveness using MR imaging in a rabbit model of anterior uveitis. *Exp Eye Res*. 2002;74:483–491.
16. Duong TQ, Pardue MT, Thule PM, et al. Layer-specific anatomical, physiological and functional MRI of the retina. *NMR Biomed*. 2008;21:978–996.
17. Bearer EL, Falzone TL, Zhang X, Biris O, Rasin A, Jacobs RE. Role of neuronal activity and kinesin on tract tracing by manganese-enhanced MRI (MEMRI). *Neuroimage*. 2007;37:S37–S46.
18. Pautler RG, Silva AC, Koretsky AP. In vivo neuronal tract tracing using manganese-enhanced magnetic resonance imaging. *Magn Reson Med*. 1998;40:740–748.
19. Bissig D, Berkowitz BA. Same-session functional assessment of rat retina and brain with manganese-enhanced MRI. *Neuroimage*. 2011;58:749–760.
20. Chan KC, Fan SJ, Zhou IY, Wu EX. In vivo chromium-enhanced MRI of the retina. *Magn Reson Med*. 2012;68:1202–1210.
21. Zhou IY, Cheung MM, Lau C, Chan KC, Wu EX. Balanced steady-state free precession fMRI with intravascular susceptibility contrast agent. *Magn Reson Med*. 2012;68:65–73.
22. Berkowitz BA, Roberto KA, Penn JS. The vitreous protein concentration is increased prior to neovascularization in experimental ROP. *Curr Eye Res*. 1998;17:218–221.
23. Chan KC, Fu QL, Guo H, So KF, Wu EX. GD-DTPA enhanced MRI of ocular transport in a rat model of chronic glaucoma. *Exp Eye Res*. 2008;87:334–341.
24. Ho LC, Conner IP, Do CW, et al. In vivo assessment of aqueous humor dynamics upon chronic ocular hypertension and hypotensive drug treatment using gadolinium-enhanced MRI. *Invest Ophthalmol Vis Sci*. 2014;55:3747–3757.
25. Watanabe T, Michaelis T, Frahm J. Mapping of retinal projections in the living rat using high-resolution 3D gradient-echo MRI with Mn2+-induced contrast. *Magn Reson Med*. 2001;46:424–429.
26. Thuen M, Singstad TE, Pedersen TB, et al. Manganese-enhanced MRI of the optic visual pathway and optic nerve injury in adult rats. *J Magn Reson Imaging*. 2005;22:492–500.
27. Chan KC, Li J, Kau P, et al. In vivo retinotopic mapping of superior colliculus using manganese-enhanced magnetic resonance imaging. *Neuroimage*. 2011;54:389–395.
28. Chan KC, Fu QL, Hui ES, So KF, Wu EX. Evaluation of the retina and optic nerve in a rat model of chronic glaucoma using in vivo manganese-enhanced magnetic resonance imaging. *Neuroimage*. 2008;40:1166–1174.
29. Chan KC, Fan SJ, Chan RW, Cheng JS, Zhou IY, Wu EX. In vivo visuotopic brain mapping with manganese-enhanced MRI and resting-state functional connectivity MRI. *Neuroimage*. 2014;90:235–245.
30. Beaulieu C. The basis of anisotropic water diffusion in the nervous system—a technical review. *NMR Biomed*. 2002;15:435–455.
31. Pierpaoli C, Barnett A, Pajevic S, et al. Water diffusion changes in Wallerian degeneration and their dependence on white matter architecture. *Neuroimage*. 2001;13:1174–1185.
32. Chan KC, Cheng JS, Fan S, Zhou IY, Yang J, Wu EX. In vivo evaluation of retinal and callosal projections in early postnatal development and plasticity using manganese-enhanced MRI and diffusion tensor imaging. *Neuroimage*. 2012;59:2274–2283.
33. Song SK, Sun SW, Ju WK, Lin SJ, Cross AH, Neufeld AH. Diffusion tensor imaging detects and differentiates axon and myelin degeneration in mouse optic nerve after retinal ischemia. *Neuroimage*. 2003;20:1714–1722.
34. Sun SW, Liang HF, Cross AH, Song SK. Evolving Wallerian degeneration after transient retinal ischemia in mice characterized by diffusion tensor imaging. *Neuroimage*. 2008;40:1–10.
35. Chan KC, Khong PL, Lau HF, Cheung PT, Wu EX. Late measures of microstructural alterations in severe neonatal hypoxic-ischemic encephalopathy by MR diffusion tensor imaging. *Int J Dev Neurosci*. 2009;27:607–615.
36. Chan KC, Xing KK, Cheung MM, Zhou IY, Wu EX. Functional MRI of postnatal visual development in normal and hypoxic-ischemic-injured superior colliculi. *Neuroimage*. 2010;49:2013–2020.
37. Kondo Y, Takada M, Honda Y, Mizuno N. Bilateral projections of single retinal ganglion cells to the lateral geniculate nuclei and superior colliculi in the albino rat. *Brain Res*. 1993;608:204–215.
38. Liu M, Duggan J, Salt TE, Cordeiro MF. Dendritic changes in visual pathways in glaucoma and other neurodegenerative conditions. *Exp Eye Res*. 2011;92:244–250.
39. Paxinos G, Watson C. *The Rat Brain in Stereotaxic Coordinates*. 6th ed. Amsterdam: Elsevier; 2007.
40. Li G, Kiel JW, Cardenas DP, De La Garza BH, Duong TQ. Postocclusive reactive hyperemia occurs in the rat retinal circulation but not in the choroid. *Invest Ophthalmol Vis Sci*. 2013;54:5123–5131.
41. Watanabe T, Tammer R, Boretius S, Frahm J, Michaelis T. Chromium(VI) as a novel MRI contrast agent for cerebral white matter: preliminary results in mouse brain in vivo. *Magn Reson Med*. 2006;56:1–6.
42. Dortch RD, Apker GA, Valentine WM, Lai B, Does MD. Compartment-specific enhancement of white matter and nerve ex vivo using chromium. *Magn Reson Med*. 2010;64:688–697.
43. Zhang X, Bearer EL, Perles-Barbacaru AT, Jacobs RE. Increased anatomical detail by in vitro MR microscopy with a modified Golgi impregnation method. *Magn Reson Med*. 2010;63:1391–1397.
44. Njie-Mbye YF, Kulkarni-Chitnis M, Opere CA, Barrett A, Ohia SE. Lipid peroxidation: pathophysiological and pharmacological implications in the eye. *Front Physiol*. 2013;4:366.

Investigative Ophthalmology & Visual Science

45. Li SY, Fu ZJ, Lo AC. Hypoxia-induced oxidative stress in ischemic retinopathy. *Oxid Med Cell Longev*. 2012;2012:426769.
46. Osborne NN, Casson RJ, Wood JP, Chidlow G, Graham M, Melena J. Retinal ischemia: mechanisms of damage and potential therapeutic strategies. *Prog Retin Eye Res*. 2004;23:91–147.
47. Wang Y, Wang Q, Haldar JP, et al. Quantification of increased cellularity during inflammatory demyelination. *Brain*. 2011;134:3590–3601.
48. Wang X, Cusick MF, Wang Y, et al. Diffusion basis spectrum imaging detects and distinguishes coexisting subclinical inflammation, demyelination and axonal injury in experimental autoimmune encephalomyelitis mice. *NMR Biomed*. 2014;27:843–852.
49. Chiang CW, Wang Y, Sun P, et al. Quantifying white matter tract diffusion parameters in the presence of increased extra-fiber cellularity and vasogenic edema. *Neuroimage*. 2014;101:310–319.
50. Petruno SK, Clark RE, Reinagel P. Evidence that primary visual cortex is required for image, orientation, and motion discrimination by rats. *PLoS One*. 2013;8:e56543.
51. Cowey A, Alexander I, Stoerig P. Transneuronal retrograde degeneration of retinal ganglion cells and optic tract in hemianopic monkeys and humans. *Brain*. 2011;134:2149–2157.
52. Park HY, Park YG, Cho AH, Park CK. Transneuronal retrograde degeneration of the retinal ganglion cells in patients with cerebral infarction. *Ophthalmology*. 2013;120:1292–1299.
53. Yamashita T, Miki A, Iguchi Y, Kimura K, Maeda F, Kiryu J. Reduced retinal ganglion cell complex thickness in patients with posterior cerebral artery infarction detected using spectral-domain optical coherence tomography. *Jpn J Ophthalmol*. 2012;56:502–510.
54. Boire D, Theoret H, Herbin M, Casanova C, Ptito M. Retinogeniculate projections following early cerebral hemispherectomy in the vervet monkey. *Exp Brain Res*. 2000;135:373–381.
55. Werth R. Cerebral blindness and plasticity of the visual system in children. A review of visual capacities in patients with occipital lesions, hemispherectomy or hydranencephaly. *Restor Neurol Neurosci*. 2008;26:377–389.
56. Werth R, Seelos K. Restitution of visual functions in cerebrally blind children. *Neuropsychologia*. 2005;43:2011–2023.
57. Werth R. Residual visual function after loss of both cerebral hemispheres in infancy. *Invest Ophthalmol Vis Sci*. 2007;48:3098–3106.
58. Werth R. Visual functions without the occipital lobe or after cerebral hemispherectomy in infancy. *Eur J Neurosci*. 2006;24:2932–2944.
59. Ptito A, Leh SE. Neural substrates of blindsight after hemispherectomy. *Neuroscientist*. 2007;13:506–518.
60. Wessinger CM, Fendrich R, Ptito A, Villemure JG, Gazzaniga MS. Residual vision with awareness in the field contralateral to a partial or complete functional hemispherectomy. *Neuropsychologia*. 1996;34:1129–1137.
61. Douglas RM, Alam NM, Silver BD, McGill TJ, Tschetter WW, Prusky GT. Independent visual threshold measurements in the two eyes of freely moving rats and mice using a virtual-reality optokinetic system. *Vis Neurosci*. 2005;22:677–684.
62. Prusky GT, Alam NM, Beekman S, Douglas RM. Rapid quantification of adult and developing mouse spatial vision using a virtual optomotor system. *Invest Ophthalmol Vis Sci*. 2004;45:4611–4616.
63. Weber AJ, Viswanathan S, Ramanathan C, Harman CD. Combined application of BDNF to the eye and brain enhances ganglion cell survival and function in the cat after optic nerve injury. *Invest Ophthalmol Vis Sci*. 2010;51:327–334.
64. Hui ES, Cheung MM, Chan KC, Wu EX. B-value dependence of DTI quantitation and sensitivity in detecting neural tissue changes. *Neuroimage*. 2010;49:2366–2374.
65. Hui ES, Fieremans E, Jensen JH, et al. Stroke assessment with diffusional kurtosis imaging. *Stroke*. 2012;43:2968–2973.
66. Hui ES, Du F, Huang S, Shen Q, Duong TQ. Spatiotemporal dynamics of diffusional kurtosis, mean diffusivity and perfusion changes in experimental stroke. *Brain Res*. 2012;1451:100–109.
67. Li G, Kiel JW, Cardenas DP, De La Garza BH, Duong TQ. Postocclusive reactive hyperemia occurs in the rat retinal circulation but not in the choroid. *Invest Ophthalmol Vis Sci*. 2013;54:5123–5131.
68. Shih YY, De la Garza BH, Muir ER, et al. Lamina-specific functional MRI of retinal and choroidal responses to visual stimuli. *Invest Ophthalmol Vis Sci*. 2011;52:5303–5310.
69. Van Camp N, Verhoye M, De Zeeuw CI, van der Linden A. Light stimulus frequency dependence of activity in the rat visual system as studied with high-resolution BOLD fMRI. *J Neurophysiol*. 2006;95:3164–3170.
70. Pawela CP, Hudetz AG, Ward BD, et al. Modeling of region-specific fMRI BOLD neurovascular response functions in rat brain reveals residual differences that correlate with the differences in regional evoked potentials. *Neuroimage*. 2008;41:525–534.
71. van de Looij Y, Chatagner A, Quairiaux C, Gruetter R, Huppi PS, Sizonenko SV. Multi-modal assessment of long-term erythropoietin treatment after neonatal hypoxic-ischemic injury in rat brain. *PLoS One*. 2014;9:e95643.
72. Macri MA, D'Alessandro N, Di Giulio C, et al. Regional changes in the metabolite profile after long-term hypoxia-ischemia in brains of young and aged rats: a quantitative proton MRS study. *Neurobiol Aging*. 2006;27:98–104.
73. Chan KC, So KF, Wu EX. Proton magnetic resonance spectroscopy revealed choline reduction in the visual cortex in an experimental model of chronic glaucoma. *Exp Eye Res*. 2009;88:65–70.
74. Seo H, Lim KH, Choi JH, Jeong SM. Similar neuroprotective effects of ischemic and hypoxic preconditioning on hypoxia-ischemia in the neonatal rat: a proton MRS study. *Int J Dev Neurosci*. 2013;31:616–623.

Investigative Ophthalmology & Visual Science